physica status solidi b
www.pss-b.com

Stacking Faults and Short-Range Magnetic Correlations in Single Crystal $Y_5Ru_2O_{12}$: A Structure with $Ru^{+4.5}$ One-Dimensional Chains

Liurukara D. Sanjeewa, Yaohua Liu, Jie Xing, Randy S. Fishman, Mudithangani T. K. Kolambage, Michael A. McGuire, Colin D. McMillen, Joseph W. Kolis,* and Athena S. Sefat*

The synthesis, structure, and physical properties of $Y_5Ru_2O_{12}$, a new member of the $Ln_5B_2O_{12}$ class (Ln = lanthanide, B = Ru, Re, Mo) are reported. Single crystals of $Y_5Ru_2O_{12}$ are synthesized using a high-temperature, high-pressure (700 °C, 200 MPa) hydrothermal method. The structure features edge-sharing Ru—O—Ru 1D chains of distorted RuO_6 octahedra. The YO_n ($n = 6$ and 7) polyhedral groups bridge Ru—O—Ru chains across the unit cell by forming a complex 3D structure. The Ru—O—Ru chains contain alternating shorter and longer Ru—Ru distances along the chain. Single crystal neutron diffraction shows streak-like diffuse scattering along the *H*-direction, due to stacking faults. Temperature-dependent anisotropic magnetic measurements reveal a broad feature over a wide temperature range, with a maximum at ≈70 K indicating potential short-range ordering, with canted antiferromagnetic behavior below 30 K. The dominant magnetic interactions are antiferromagnetic with a large negative Weiss temperature $\theta \approx -200$ K. The compound has an effective magnetic moment that is anomalously large for this class of compounds (≈4 μ_B Ru^{-1}), and a phenomenological spin Hamiltonian describing the unusual anisotropic magnetization of $Y_5Ru_2O_{12}$ is proposed.

1. Introduction

The magnetism of 4*d* and 5*d* metal oxides is interesting due to the presence of spin–orbital (S–O) coupling that is much stronger than in 3*d* transition metal compounds.[1] The ligand field effects are also strong in these compounds, comparable in value to the first row 3*d* ions, making the 4*d* and 5*d* metal ions unique relative to both the 3*d* ions and the rare earth ions. Despite these intriguing facts, the 4*d* and 5*d* metal ions are significantly less studied than either the 3*d* metal ions or the lanthanides. In particular, ruthenium displays an exceptionally rich range of unusual magnetic and transport properties[2,3] and can exist in several oxidation states, including Ru^{3+}, Ru^{4+}, Ru^{5+}, and Ru^{7+}, where Ru^{4+} is the most common oxidation state.[4–10] For example, Sr_2RuO_4 is a superconductor below $T_c = 0.93$ K,[6] $SrRu_2O_6$ is a high-temperature antiferromagnet ($T_N = 565$ K),[11] $SrRuO_3$ is a ferromagnet below $T_C = 163$ K,[12] and $La_4Ru_6O_{19}$[13] is a non-Fermi liquid.

As one illustration of the potential of these materials, Ru compounds in the 6H perovskite type structures with a common formula of $Ba_3ARu_2O_9$ (*A* = In, La–Lu, Y, Zn, Sr, Na) are good examples of the rich physical properties that can be observed in ruthenates.[14–22] The general structure contains 2D triangular layers of face-sharing octahedra forming Ru_2O_9 dimers, and can range from relatively high ($P6_3/mmc$) to lower (monoclinic) symmetry, or exhibit structural transitions ($Ba_3NaRu_2O_9$: $P6_3/mmc$ to $P2/c$ at 210 K)[17,18] or distortions ($Ba_3BiRu_2O_9$: structural dimerization at 176 K[21]) with temperature. The oxidation state of Ru in 6H compounds depends on the nature of the A-site cation, so the magnetic behavior varies widely. When the A-site cation is divalent and nonmagnetic, for example, in $Ba_3CaRu_2O_9$ where Ru is 5+,[23] a broad hump in magnetic susceptibility data is shown without long-range ordering, and spin liquid behavior was predicted in $Ba_3ZnRu_2O_9$ by Terasaki et al. with no ordering down to 37 mK.[24] In contrast, when A^{2+} contains open shell *d* electrons (e.g., $Ba_3CoRu_2O_9$ and $Ba_3NiRu_2O_9$), antiferromagnetic ordering occurs at lower

Dr. L. D. Sanjeewa, Dr. J. Xing, Dr. R. S. Fishman, Dr. M. A. McGuire, Dr. A. S. Sefat
Materials Science and Technology Division
Oak Ridge National Laboratory
Oak Ridge, TN 37831, USA
E-mail: sanjeewald@ornl.gov

Dr. Y. Liu
Neutron Scattering Division
Oak Ridge National Laboratory
Oak Ridge, TN 37831, USA

Dr. M. T. K. Kolambage, Dr. C. D. McMillen, Prof. J. W. Kolis
Department of Chemistry
Center for Optical Materials Science and Engineering Technologies (COMSET)
Clemson University
Clemson, SC 29634-0973, USA
E-mail: kjoseph@clemson.edu

The ORCID identification number(s) for the author(s) of this article can be found under https://doi.org/10.1002/pssb.202000197.

DOI: 10.1002/pssb.202000197

temperatures.[16] When the A-site cation is trivalent, ferromagnetic Ru-spin dimers were observed in $Ba_3ARu_2O_9$ (A = La, Nd, and Y) using neutron powder diffraction,[15] while $Ba_3CeRu_2O_9$ displays no evidence of long-range magnetic ordering down to 0.3 K.[20] This extensive list of different properties justifies further development of the chemistry of metal ion ruthenates.

The synthesis of ruthenates typically uses high-temperature solid state ($T > 1200\,^{\circ}C$) reactions that most often yield products in the form of powders.[14–19] This approach has some limitations, in that the high temperatures can volatilize components and potentially lead to nonstoichiometry, lattice defects, and site occupancy disorder. These problems can cause difficulty in the accurate determination of physical properties. Recently, our group has used high-temperature hydrothermal growth as a route to single crystals with minimal lattice defects and site disorder. We found that hydrothermal reactions performed at 700 °C at pressures of ≈200 MPa can lead to a wide range of defect-free refractory rare-earth-containing oxides.[25–34] The work was recently extended to a series of lanthanide rhenates such as $LnRe_2O_7(OH)$ (Ln = Pr and Nd) and $Ln_4Re_2O_{11}$ (Ln = Eu and Tb),[34] as well as a series of rare-earth ruthenates.[35] In addition, a low temperature hydrothermal method (200 °C) has been used to synthesize powders of $Ca_{1.5}Ru_2O_7$, $SrRu_2O_6$, and $Ba_2Ru_3O_9(OH)$.[8,9]

In this article, we target hydrothermally synthesized $Y_5Ru_2O_{12}$ as a protype test compound for detailed magnetic study of rare-earth ruthenates.[36–38] These compounds possess the unusual feature of 1D chains made from either 4*d* or 5*d* transition metal cations with an average oxidation state of 4.5, reminiscent of the 6H perovskites mentioned earlier. The magnetism of $Ln_5B_2O_{12}$ (B = Mo, Ru, Re) compounds has attracted much interest due to the presence of mixed valent 1D chains of the 4*d* or 5*d* ions.[36–39] The compounds are made more interesting by the presence of alternating shorter and longer B—B (Ru—Ru, Re—Re, or Mo—Mo) distances. The intermediate valence state of Ru with alternating bond distances leads to complex magnetic behavior and these properties are made harder to understand due to the presence of lanthanide ions that can have large magnetic moments themselves. It has been suggested that these shorter distances are the result of a B—B bonds, which leave one unpaired electron per B_2O_{10} dimer, resulting in a spin value of $S = ½$ per dimer unit. In 2009, Bharathy et al. reported a series of ruthenate analogs of $Ln_5Ru_2O_{12}$ compounds and reported some magnetic data;[36] however, all of examples contained an open-shell rare-earth ion, so the magnetic properties were dominated by the lanthanide ions.

In this work, we focus on $Y_5Ru_2O_{12}$ as our initial target material because Y^{3+} contains no unpaired electrons, allowing us to explore the magnetic properties that arise solely from the 1D Ru—O—Ru chains. We note that high-temperature synthesis and magnetic properties of $Y_5Re_2O_{12}$ and $Y_5Mo_2O_{12}$ have been reported previously,[37,38] although they are limited only to polycrystalline samples and the contrast in their magnetic behavior with the ruthenate analogs are discussed herein. In this work, we describe a high-temperature, high-pressure hydrothermal synthesis of large, high-quality $Y_5Ru_2O_{12}$ single crystals and this important development provides two significant reasons to investigate this unusual system. First, the rare-earth site is magnetically silent, meaning that the only magnetic signal will result from the ruthenium oxo chains. Second, the growth of sufficiently large single crystals allows for single crystal neutron diffraction as well as the orientation of the crystal in a magnetic field to measure anisotropic magnetic behavior. In this article, we discuss the structure characterization using single crystal X-ray diffraction as well as the anisotropic magnetic properties of $Y_5Ru_2O_{12}$ determined using optically aligned single crystals with the magnetic field parallel and perpendicular to the 1D Ru chains. We also perform single crystal neutron diffraction and observe diffuse scattering associated with stacking faults due to the defect structure in $Y_5Ru_2O_{12}$. Further, we describe the observed anisotropic magnetic properties using a Hamiltonian calculation.

2. Experimental Section

2.1. Hydrothermal Synthesis of $Y_5Ru_2O_{12}$

Single crystals of $Y_5Ru_2O_{12}$ were grown using a high-temperature and high-pressure hydrothermal method. Reactions were performed in 2.75 in. long silver tubes having an inner diameter of 0.375 in. In a typical reaction, Y_2O_3 (Alfa Aesar, 99.9%) and RuO_2 (Alfa Aesar, 99.9%) were used in a 5:4 stoichiometric ratio. Here a total of 0.4 g of Y_2O_3 (0.2718 g) and RuO_2 (0.1282 g) was loaded into a silver tube with 0.8 mL of 30 M KOH. The silver ampules were welded shut and placed in a Tuttle-seal autoclave that was filled with water to provide appropriate counterpressure. The autoclaves were heated to 700 °C for two weeks, reaching an average pressure of 200 MPa, utilizing ceramic band heaters. Black columnar crystals (Figure S1, Supporting Information) were recovered by washing with deionized water using suction filtration.

2.2. X-Ray Diffraction

The single crystal structure was characterized using a Bruker D8 Venture diffractometer equipped with a Mo Kα microfocus source and Photon 100 CMOS detector. All data were collected at room temperature using phi and omega scans. Data collection, processing, and scaling (multiscan, SADABS) were performed using the Apex3 software suite.[40] The structures were solved by direct methods and refined by full-matrix least-squares on F^2 using SHELXTL.[41] All atoms were refined anisotropically. The crystal analyzed exhibited positional disorder of the Ru(1), Y(3), O(3), and O(4) sites, as often occurs in these systems.[36] The occupancy of the disordered components was freely refined, with the major component found to be 95.5% occupancy, and the minor component 4.5% occupancy. Crystallographic data are summarized in **Table 1**, and selected interatomic distances for the major disordered component are provided in **Table 2**.

2.3. Magnetic Property Characterization

The temperature- and field-dependent magnetic measurements were conducted using a SQUID magnetometer (Quantum Design MPMS). Here, several single crystals were aligned

Table 1. Crystallographic data of $Y_5Ru_2O_{12}$ determined by single crystal X-ray diffraction.

Empirical formula	$Y_5Ru_2O_{12}$
Formula weight [g mol^{-1}]	838.69
Crystal dimensions [mm]	0.10 × 0.04 × 0.02
Crystal system	Monoclinic
Space group, Z	$C2/m$ (no.12), 2
T [K]	298
a [Å]	12.3217(13)
b [Å]	5.8121(5)
c [Å]	7.2918(8)
β [°]	107.369(4)
Volume [Å^3]	498.39(9)
D (calc.) [g cm^{-3}]	5.589
μ (Mo Kα) [mm^{-1}]	31.770
F(000)	758
T_{max}, T_{min}	1.0000, 0.7855
θ range	2.93–25.50
Reflections collected	4734
Data/restraints/parameters	515/12/66
Final R [$I > 2\sigma(I)$] R_1, R_{w2}	0.0284, 0.0517
Final R (all data) R_1, R_{w2}	0.0338, 0.0529
GoF	1.125
Largest diff. peak/hole [e/Å^3]	0.938/−1.109

Table 2. Selected bond lengths (Å) of $Y_5Ru_2O_{12}$.

$Ru(1)O_6$		$Y(2)O_7$	
Ru(1)—O(2) × 2	1.927(4)	Y(2)—O(1) × 2	2.319(4)
Ru(1)—O(3) × 2	1.962(5)	Y(2)—O(1) × 2	2.323(4)
Ru(1)—O(4) × 2	2.043(4)	Y(2)—O(2) × 2	2.369(4)
		Y(2)—O(4) × 1	2.360(6)
$Y(1)O_7$		$Y(3)O_6$	
Y(1)—O(1) × 2	2.317(4)	Y(3)—O(1) × 4	2.308(4)
Y(1)—O(2) × 2	2.392(4)	Y(3)—O(3) × 2	2.249(6)
Y(1)—O(2) × 2	2.282(4)		
Y(1)—O(4)	2.315(6)		
Ru(1)—Ru(1)	2.755(3)		
Ru(1)—Ru(1)	3.057(3)		

along the direction of $[RuO_4]_\infty$ chain propagation (i.e., the crystallographic b-axis), enabling the direction of the applied field to be varied relative to the direction of chain propagation. The temperature-dependent static susceptibility was measured in the temperature region of 2–350 K under 10 kOe applied magnetic field. Isothermal magnetization was performed at both 2 and 300 K, up to the applied magnetic field of 60 kOe.[42]

2.4. Single Crystal Neutron Diffraction

Low-temperature single crystal neutron diffraction experiments were conducted at the CORELLI spectrometer at the Spallation Neutron Source (SNS) at Oak Ridge National Laboratory. CORELLI is a quasi-Laue time-of-flight instrument with large 2D detector coverage, and is optimized for identifying weak scattering features, such as broad diffuse scattering, over a large reciprocal space. Its unique optical component, a correlation chopper, allows for the extraction of both an energy-integrated scattering signal and the elastic-only scattering signal at the same time. The size of the crystals used in the diffraction experiments was ≈1.5 × 0.5 × 0.5 mm^3. The data were collected during two separate runs at temperatures between 1.5 and 110 K. In the first run, the data were collected between 6 and 110 K, using a low-background close-cycled refrigerator to search for magnetic diffuse scattering associated with short-range magnetic ordering (see magnetic property discussion). In the second run, the data were collected at 1.5 and 12 K using a liquid helium research dewar (orange cryostat) to search for magnetic Bragg peak scattering. Experiments were conducted by rotating the sample through a 180° range with a 2° step at each temperature. The Mantid package was used for data reduction, including Lorentz and spectrum corrections.[43,44]

3. Results and Discussion

3.1. Crystal Structure of $Y_5Ru_2O_{12}$

The compound $Y_5Ru_2O_{12}$ was synthesized using a high-temperature, high-pressure hydrothermal method and could be isolated as large, well-formed single crystals suitable for oriented anisotropic measurements and single crystal neutron measurements. It crystallizes in the monoclinic space group of $C2/m$ (no.12). Single crystal X-ray diffraction provided unit cell parameters of $a = 12.3217(13)$ Å, $b = 5.8121(5)$ Å, $c = 7.2918(8)$ Å, $\beta = 107.369(4)°$, $V = 498.39(9)$ Å^3, and $Z = 2$. A summary of the crystallographic parameters and bond distances is provided in Table 1 and 2, respectively. The detailed crystallographic data, including Wyckoff positions, refined occupancies, and thermal parameters, are given in Table S1, Supporting Information. As mentioned previously, $Y_5Ru_2O_{12}$ is another addition to the $Ln_5B_2O_{12}$ family of compounds where Ln is a lanthanide element (La–Lu and Y) and B can be either 4d or 5d transition metals such as Mo, Ru, and Re. The $Ln_5B_2O_{12}$ family possesses a complex 3D structure made from LnO_n ($n = 6$, 7) polyhedra and BO_6 octahedra. In this study, we were able to grow good-sized single crystals of $Y_5Ru_2O_{12}$ and determine the structure using single crystal X-ray diffraction and single crystal neutron diffraction. After this careful structure analysis, we confirmed that hydrothermally grown $Y_5Ru_2O_{12}$ crystallizes in $C2/m$, similar to the $Ln_5Ru_2O_{12}$ (Ln = Pr, Nd, Sm–Tb) series reported by Bharathy et al. in 2009. It is noteworthy to mention that Bharathy et al. observed a twinned and disordered structures for the $Ln_5Ru_2O_{12}$ (Ln = Eu, Gd, and Tb) compounds (but *not* $Pr_5Ru_2O_{12}$) and provided a detailed crystal structure refinement.[36] According to the Bharathy et al.'s report, the $Pr_5Ru_2O_{12}$ structure can be solved as an ideal disorder free structure; however, Eu, Gd, and Tb members possess disorders/

defects in Ln, Ru, and O sites, which create a (0,0,1/2) shift in the unit cell compared to the disorder-free structure. A similar disordered structure was also observed in $Y_5Re_2O_{12}$,[37] and we also observed a similar disorder/defect structure in $Y_5Ru_2O_{12}$ (though without a twin contribution). Such disordered $Ln_5Ru_2O_{12}$ structures can produce stacking faults, which was previously observed in high resolution transmission electron microscopy (HRTEM) images,[36] and similar stacking faults were observed here in $Y_5Ru_2O_{12}$ from single crystal neutron diffraction, as discussed below.

The partial polyhedral structure of $Y_5Ru_2O_{12}$ is shown in **Figure 1**a. The 1D Ru—O—Ru chains propagate along the *b*-axis and these chains are interconnected via the thicker Y—O—Y sublattice to form a complex 3D structure. Figure 1b displays the 1D Ru—O—Ru chains made from edge-sharing RuO_6 octahedra via two O(3) and two O(4) atoms. The Ru—O bond lengths range from 1.927(4) to 2.043(5) Å, indicating a degree of distortion within the RuO_6 octahedron. Edge-sharing Ru(1)—O(4) and Ru(1)—O(3) bond distances are 2.043(5) and 1.962(5) Å, respectively, that alternate along the Ru—O—Ru chain. The alternating shorter and longer Ru—O bonds also create alternating Ru—Ru distances (2.755(3) and 3.057(3) Å) along the chain. This behavior has been observed in all $Ln_5B_2O_{12}$ compounds and both the alternating Ru—Ru distances and the Ru—O bond lengths fall within the range previously observed for the $Ln_5Ru_2O_{12}$ series.[36] The Ru—O—Ru chains interconnect with Y(1)O_7 polyhedra along the *c*-axis, forming 2D slabs along the *bc*-plane. Y(2)O_7 and Y(3)O_6 form a complex Y—O—Y sublattice around the Y(1)—O—Ru—O—Y(1) lattice, forming a highly condensed structure (Figure S2, Supporting Information).

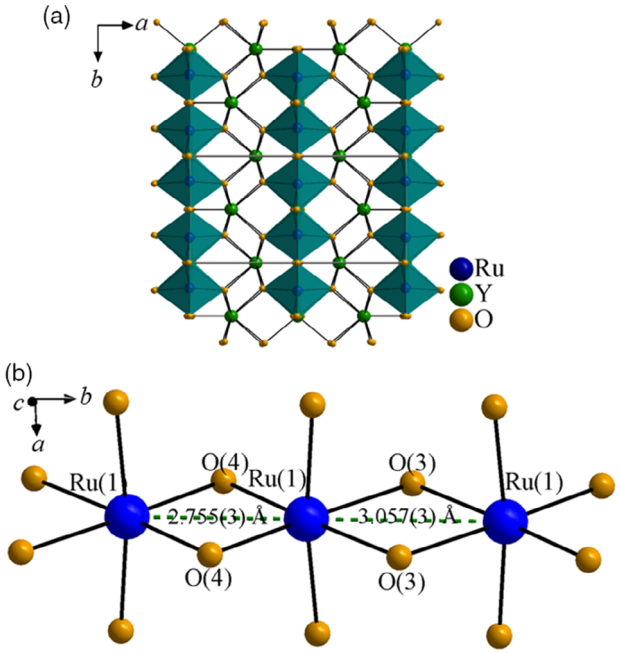

Figure 1. $Y_5Ru_2O_{12}$ structure: a) partial polyhedral view along the *ab*-plane showing the connectivity between the Y—O—Y lattice and the propagation of Ru—O—Ru chains along the *c*-axis. b) Partial structure of Ru—O—Ru chain made from edge-sharing RuO_6 octahedra along the *b*-axis via O(3) and O(4). The alternating shorter and longer Ru—Ru distance is shown by green dashed lines.

3.2. Magnetic Properties of $Y_5Ru_2O_{12}$

The anisotropic magnetic properties of $Y_5Ru_2O_{12}$ were examined and the temperature-dependent magnetic susceptibility measured in orientations both parallel and perpendicular to the

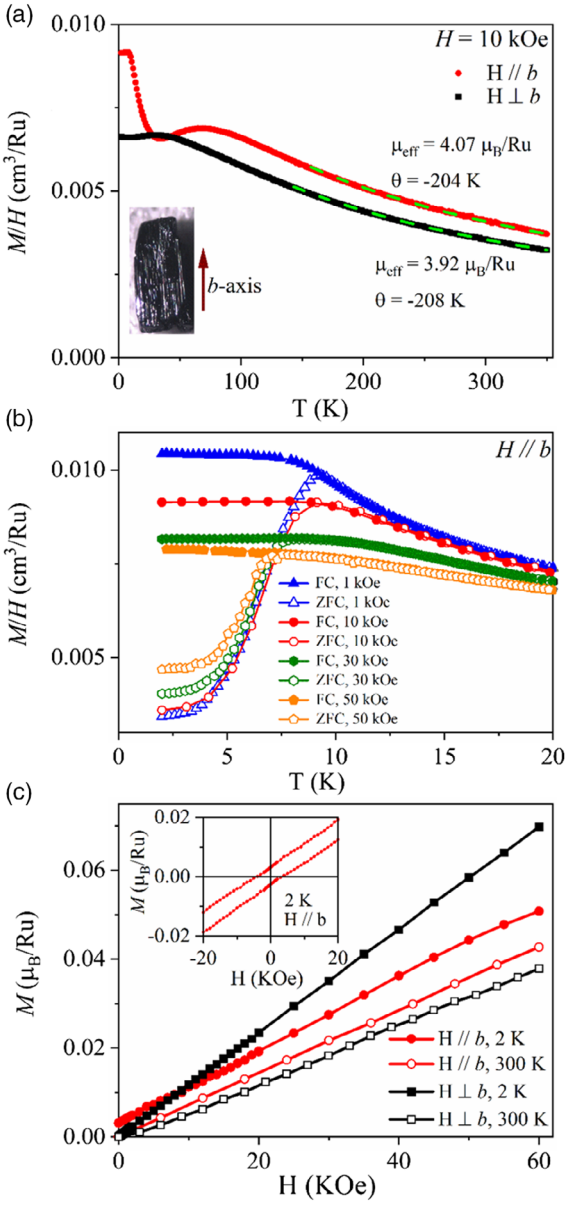

Figure 2. a) Temperature-dependent magnetic susceptibility measured along two different directions *H*//*b* (red) and *H*⊥*b* (black); the inset shows a single crystal of $Y_5Ru_2O_{12}$ with the *b*-axis oriented along the longest dimension of the crystal. b) Temperature- and field-dependent magnetic susceptibility for *H*//*b*, showing a field-dependent divergence between ZFC and FC. c) Isothermal magnetization measured along the *H*//*b* (red) and *H*⊥*b* (black) directions, showing a small remnant magnetization for *H*//*b* at 2 K, while linear behavior is found for *H*⊥*b* at room temperature.

Ru—O—Ru chain directions ($H//b$ and $H\perp b$) (**Figure 2**a). Magnetic susceptibility along the *b*-axis shows a broad hump, with a maximum at 75 K suggesting a potential short-range ordering. Upon further cooling, susceptibility starts to increase at 30 K, finally showing a long-range order at 7 K. In addition, the field cooling (FC) and zero field cooling (ZFC) show a divergence at 7 K (Figure 2b). A similar behavior was observed when the magnetic field was applied perpendicular to the chain direction (Figure S3, Supporting Information). In this case, however, the broad hump is suppressed and shifts to lower temperature (Figure 2b). The increase in susceptibility around 30 K and the presence of divergence between FC and ZFC suggests a canted antiferromagnetic nature of $Y_5Ru_2O_{12}$. Isothermal magnetization measured at 2 K with $H//b$ and $H\perp b$ is primarily linear, with some curvature at higher field for $H//b$ data. This curvature behavior could be due to a spin reorientation toward the Ru—O—Ru chain direction at a higher magnetic field. When the magnetic field is oriented along the *b*-axis, the magnetization reaches 0.05 μ_B Ru^{-1} at 60 kOe, which is much smaller than the fully magnetic moment for a $Ru^{+4.5}$ system. In addition, a small hysteresis behavior was observed in the isothermal magnetization data at 2 K for $H//b$. Overall, the results suggest that $Y_5Ru_2O_{12}$ may order antiferromagnetically with an uncompensated magnetic moment below 30 K. Magnetic susceptibility data were fitted for both directions using the Curie–Weiss law of $\chi = C/(T-\theta)$ above 100 K, and the fitted values for both $H//b$ and $H\perp b$ directions are very similar (Figure 2a). The effective magnetic moments for $H//b$ and $H\perp b$ are 4.07 and 3.92 μ_B Ru^{-1}, respectively, and the Curie–Weiss temperatures are −204 and −208 K, which suggest strong antiferromagnetic interactions between Ru atoms. Higher Curie–Weiss temperatures have been observed only in a handful of Ru-based compounds such as $Ba_3NaRu_2O_9$ ($\theta = -429$ K), $Ba_3LiRu_2O_9$ ($\theta = -634$ K), and $BaZnRu_5O_{11}$ ($\theta = -230$ K).[17,18,39] The large negative Curie–Weiss temperatures in these compounds indicate a dominant antiferromagnetic interaction between the ruthenium atoms in the magnetic lattice. However, it is important to note that there could be an uncertainty in the θ value of $Y_5Ru_2O_{12}$ due to the limited temperature range of the magnetic susceptibility experiment (2–350 K). Therefore, measuring magnetic susceptibility above 400 K and fitting the data beyond room temperature (300 K) could help to obtain a very accurate θ value for $Y_5Ru_2O_{12}$. Nevertheless, irrespective of the exact θ value a large negative Curie–Weiss temperature suggests a significant antiferromagnetic correlation in $Y_5Ru_2O_{12}$.

The $Ln_5B_2O_{12}$ family of compounds is quite unique in that it contains characteristic alternating longer and shorter distances between the B ions in an edge-sharing chain. It is suggested that these short distances are the result of metal–metal bonds, leaving one unpaired electron per B_2O_{10} dimer.[37–39,45] For example, in $Y_5Re_2O_{12}$, the average Re oxidation is +4.5, which results in 2.5 electrons per Re atom, or 5 electrons per rhenium dimer, and 4 of these electrons can be assigned to form a Re=Re double bond, leaving one unpaired electron per rhenium dimer to create an $S = 1/2$ local moment per formula unit. Similarly, the $Ln_5Mo_2O_{12}$ series in which Mo is in the formal +4.5 oxidation state contains three electrons per molybdenum dimer, generating one bond and one unpaired electron per formula unit. Thus, the spin-only effective magnetic moment (μ_{eff}) for these compounds is expected to be ≈1.73 μ_B. From previous work, the calculated magnetic moment from Curie–Weiss fits of $Lu_5Mo_2O_{15}$ and $Y_5Mo_2O_{12}$ are 1.52 and 1.70 μ_B, respectively, in good agreement with this prediction and suggesting the presence of an $S = 1/2$ state per dimer.[38] However, the measured effective magnetic moment of $Y_5Re_2O_{12}$ is only 0.31 μ_B, which is much smaller than the expected magnetic moment for $S = ½$ rhenium dimers. Moreover, $Y_5Re_2O_{12}$ displays short-range ordering with a broad hump with a maximum at 125 K.[37] By extending these studies, a series of $Ln_5Ru_2O_{12}$ compounds was prepared but the situation was complicated by the fact that the rare-earth sites in all these ruthenates were magnetically active as well.[36] In such cases, the magnetic behavior can be dominated by the unpaired *f* electrons, making the magnetism associated with $Ru^{+4.5}$ (or $S = 1/2$ ruthenium dimers) difficult to assign accurately. For example, $Eu_5Ru_2O_{12}$ and $Sm_5Ru_2O_{12}$ do not show any ordering down to 2 K, whereas $Tb_5Ru_2O_{12}$ shows long-range antiferromagnetic ordering at 7 K, making it hard to definitively confirm the presence of $S = 1/2$ Ru dimers in $Ln_5Ru_2O_{12}$ compounds.

In this study, we successfully synthesized large single crystals of $Y_5Ru_2O_{12}$, where Y^{3+} contains no unpaired electrons, so we were able to isolate the magnetic properties only associated with the ruthenium ions. As ruthenium is in a formal +4.5 oxidation state, each dimer contains seven valence *d* electrons per dimer. Assuming each Ru dimer of $Y_5Ru_2O_{12}$ is consistent with an $S = 1/2$ state, an attempt was made to fit the data using a similar method to $Y_5Re_2O_{12}$.[38] However, our magnetic data fitting does not provide any conclusive evidence for the presence of $S = 1/2$ states per ruthenium dimer. The effective magnetic moment for $Y_5Ru_2O_{12}$ (≈4 μ_B Ru^{-1}) is much larger than expected for an $S = ½$ state, which suggests that more unpaired electrons are present in the Ru chains. This scenario is difficult to explain based on localized Ru–Ru bonding in the dimers. To examine this contrast in more detail, we compare the Ru—Ru distances in $Y_5Ru_2O_{12}$ with those in the 6H perovskite structures in the literature. The presence of Ru—Ru metallic bonds was confirmed in $Ba_3MRu_2O_9$ (M = In, Lu, Y) using a wide array of experiments, including inelastic neutron scattering. The average oxidation state of Ru in the octahedra in $Ba_3MRu_2O_9$ (M = In, Lu, Y) is 4.5+ and the Ru—Ru distance is ≈2.5 Å, compared to 2.755(3) and 3.057(3) Å in $Y_5Ru_2O_{12}$.[14,20] The significantly longer Ru—Ru distance in $Y_5Ru_2O_{12}$ suggests that we could eliminate the presence of Ru—Ru metallic bonds, and therefore the $S = ½$ state, in $Y_5Ru_2O_{12}$. Further, the shorter Ru—Ru distance of $Y_5Ru_2O_{12}$ (2.755(3) Å) is comparable with the Ru—Ru distances of the 6H perovskites $Ba_3LiRu_2O_9$ and $Ba_3NaRu_2O_9$, which are 2.7482(9) and 2.768(1) Å, respectively. The average oxidation state of Ru in $Ba_3LiRu_2O_9$ and $Ba_3NaRu_2O_9$ is +5.5. A detailed study of $Ba_3NaRu_2O_9$ confirms that the relatively longer Ru—Ru distances in Ru_2O_9 dimers lead to an electron localization due to the Coulombic interactions.[17,18] In other words, $Ba_3NaRu_2O_9$ undergoes charge ordering at lower temperatures, which implies that both Ru^{5+} and Ru^{6+} cations are disordered on a single crystallographic site at room temperature but ordered separately at lower temperatures. Therefore, we postulate that $Y_5Ru_2O_{12}$ may behave very similarly to $Ba_3LiRu_2O_9$ and $Ba_3NaRu_2O_9$ compounds by having ordered Ru^{+4} ($4d^4$, $S = 1$) and Ru^{+5} ($4d^3$, $S = 3/2$) sites in the Ru—O—Ru chain. Separately ordered

Ru^{+4} and Ru^{+5} sites would have ideal spin-only effective magnetic moments of 2.87 and 3.87 μ_B, respectively, with an average of 3.37 $\mu_B\,Ru^{-1}$. This is only slightly smaller (by 16%) than the measured effective magnetic moment for $Y_5Ru_2O_{12}$, implying some possible contribution of S–O coupling. It is well known that Ru ions display a range of variations in magnetic moment from the ideal spin-only values. For example, an unusually high effective magnetic moment (4.95 μ_B) has been observed in Sr_2RuO_4 (Ru^{+4}). In this case, Ru^{+4} is assigned to a high-spin state because Ru is in a highly distorted environment because of a co-operative Jahn–Teller effect.[46,47]

Moreover, we propose a model for the spin structure in the ordered regime by using alternating isolated low spin values of $S=1$ (Ru^{+4}) and $S=3/2$ (Ru^{+5}). The exchange coupling along the shorter bond is denoted J_1, while the coupling along the longer bond is denoted J_2. Spins with $S_1=1$ occupy odd sites, while those with $S_2=3/2$ occupy even sites. Therefore, the simplest Hamiltonian can be written

$$H = -J_1 \sum_i {}_{\text{odd}}\mathbf{S}_i \cdot \mathbf{S}_{i+1} - J_2 \sum_i {}_{\text{even}}\mathbf{S}_i \cdot \mathbf{S}_{i+1} + K \sum_i {}_{\text{odd}}(\mathbf{S}_i \cdot b)^2 - g\mu_B H \sum_i \mathbf{S}_i \cdot \mathbf{m} \quad (1)$$

where spins with $S_1=1$ have odd i and spins with $S_2=3/2$ have even i. The field direction is given by the vector $\mathbf{m}$. The anisotropy term $K>0$ maintains the spins in the ac-plane. Because the spins are free to rotate in the ac-plane, the magnetization is smaller when the field is applied along the b-axis than when it is applied perpendicular to the b-axis. Based on a simple model of $Y_5Ru_2O_{12}$ with four spins in the unit cell (**Figure 3**), we consider two scenarios. If $J_1<0$ is antiferromagnetic, then spins 1 and 2 on the dimer will be aligned antiparallel to give a net spin of $S_{\text{dim}}=S_2-S_1=½$. However, this would produce a much smaller effective moment ($\mu_{\text{eff}}=\mu_B[S_{\text{dim}}(S_{\text{dim}}+1)]^{1/2}=0.87\,\mu_B\,Ru^{-1}$) than the observed effective moment of $\approx 4\,\mu_B\,Ru^{-1}$. Due to the uncertainty in the spin of the dimer, we shall simply assume that the magnitude of the coupling $|J_1|$ within each dimer is much stronger than the magnitude of the coupling $|J_2|$ between dimers. In that case, both J_1 and S_{dim} drop out of the predictions for the magnetization, as seen subsequently. We assume that $J_2<0$ is antiferromagnetic.

The spins on neighboring dimers are given by the classical vectors

$$\mathbf{S}_{\text{dim}\,a} = S_{\text{dim}}(\sin\phi_a \sin\theta_a, \cos\phi_a \sin\theta_a)$$
$$\mathbf{S}_{\text{dim}\,b} = S_{\text{dim}}(\sin\phi_b \sin\theta_b, \cos\phi_b \sin\theta_b) \quad (2)$$

so that ϕ_a and ϕ_b denote rotations about the b-axis, while θ_a and θ_b are the tilt angles of the spins off the b-axis. The energy per dimer is given by

$$E/N = -S_{\text{dim}}^2 J_2\{\cos\theta_a \cos\theta_b + \sin\theta_a \sin\theta_b \cos(\phi_a - \phi_b)\} + 1/2KS_{\text{dim}}^2\{\cos^2\theta_a + cos^2\theta_b\} - 1/2g\mu_B HS_{\text{dim}}\{m_a(\sin\phi_a \sin\theta_a + \sin\phi_b \sin\theta_b) + m_b(\cos\theta_a + \cos\theta_b) + m_c(\cos\phi_a \sin\theta_a + \cos\phi_b \sin\theta_b)\} \quad (3)$$

By minimizing the classical energy as a function of the four angles of the dimer spins, we find the magnetization per formula unit (one dimer) is given by

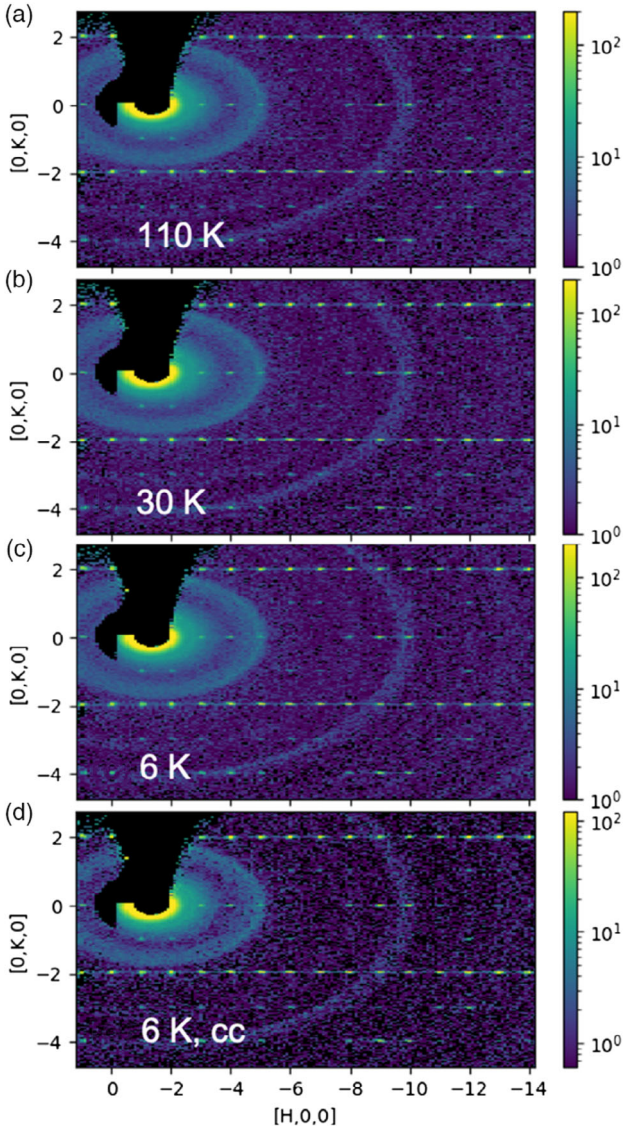

Figure 4. Temperature-dependent single crystal neutron diffraction patterns collected at a) 110 K, b) 30 K, and c,d) 6 K. The 2D slices are taken at $L=3$. a–c) Energy-integrated scattering datasets and d) elastic-only scattering dataset. A streak-like diffuse scattering can be observed at all temperatures.

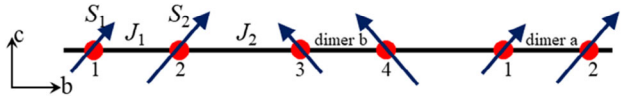

Figure 3. A simple model for $Y_5Ru_2O_{12}$ with four spins in the unit cell.

$$\frac{M}{N} = \frac{(g\mu_b)^2 H}{2(2|J_2| + K)}, \quad \mathbf{m}//\mathbf{b}$$
$$\frac{M}{N} = \frac{(g\mu_b)^2 H}{4|J_2|}, \quad \mathbf{m} \perp \mathbf{b} \tag{4}$$

Using the observed magnetizations at 5 T of 0.089 and 0.116 μ_B f.u.$^{-1}$ for fields parallel and perpendicular to **b**, respectively, and assuming that $g = 2$, we obtain $|J_2| = 2.5$ meV and $K = 1.5$ meV.

3.3. Single Crystal Neutron Diffraction

To further investigate the nuclear and the magnetic structure, we collected single crystal neutron diffraction data at different temperatures between 1.5 and 100 K. We did not, however, find any new Bragg-peak-like features or any significant enhancement in peak intensities that may be associated with the long-range magnetic ordering, which could be due to the relatively small sample size used in our experiment. Interestingly, streak-like diffuse scattering features were observed in the samples at all temperatures collected, indicating some local disorder in the nuclear structure. There are clearly streak-like diffuse scattering features along the H direction of diffraction patterns slices at the [H K 3] plane at 110, 30, and 6 K, which barely show any temperature dependence (**Figure 4**). The elastic scattering signal shows essentially the same pattern as the energy-integrated scattering signal, indicating that such scattering is of static origin. These streak-like features usually come from coherent planar defects. There are several notable features of these diffuse streaks (Figure 4d). The diffuse streak along H is visible for odd L but not for even L (**Figure 5**). For odd L the streak is more pronounced at even K positions and less pronounced at odd K positions.

The reported structures for $Ln_5Ru_2O_{12}$ compounds, as mentioned previously, contain a defect structure consisting of stacking faults.[36] In our case, **Figure 6**a displays a comparison of disorder-free and average disordered (Figure 6b) $Y_5Ru_2O_{12}$ structures. By projecting the crystal structure into the *ac*-plane, a disorder-free $Y_5Ru_2O_{12}$ (similar to $Pr_5Ru_2O_{12}$ in Fulle et al.[32]) structure can be viewed as alternative stacking of two identical layers with an interlayer displacement vector $\mathbf{t}_{12} = \mathbf{t}_{21} = [½, ½, 0]$ (Figure 4a). A stacking fault forms if there is a glide along the *c*-axis with a shift displacement vector of [0, 0, ½] so that the interlayer displacement vector becomes $\mathbf{t}_{12'} = \mathbf{t}_{21'} = [½, ½, ½]$ between

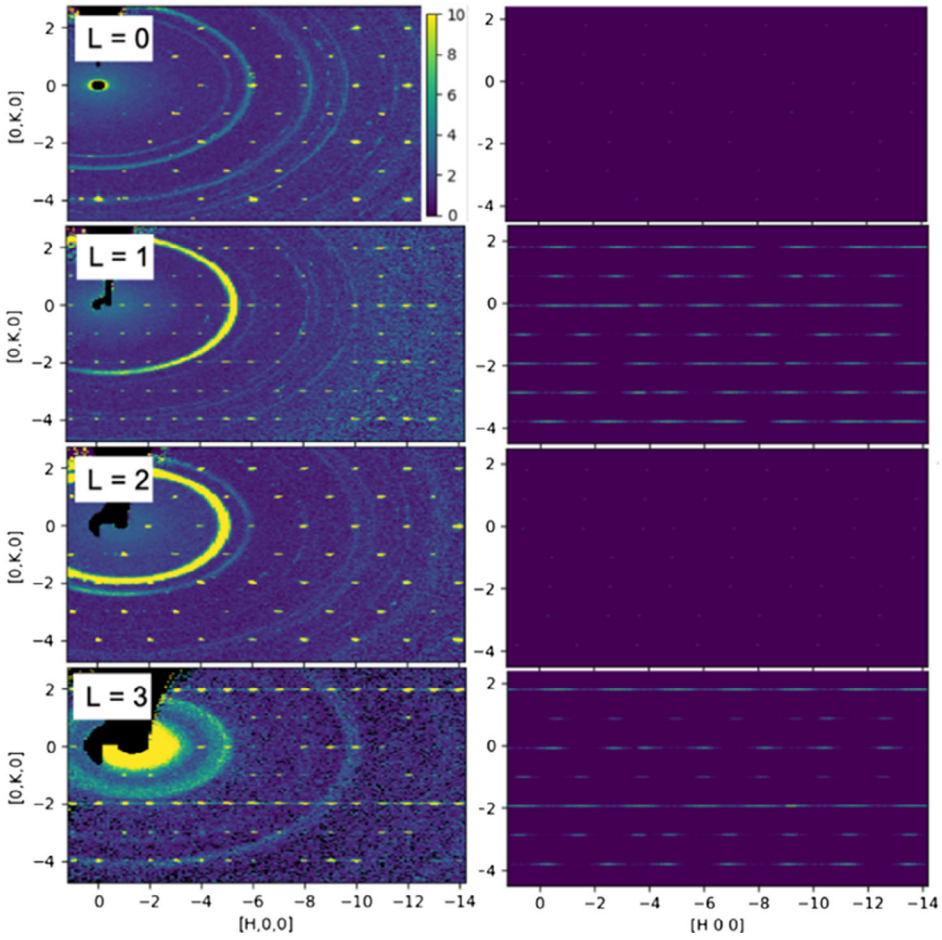

Figure 5. Comparison of the experimental data (left, 110 K), and simulations (right) of the diffuse scattering patterns for [H 0 0]–[0 K 0] plane sliced at different L. There is no significant diffuse scattering for $L = 0$ and 2 in both the experimental data and the simulations. For odd L, the streaks are more pronounced at even K positions and less pronounced at odd K positions.

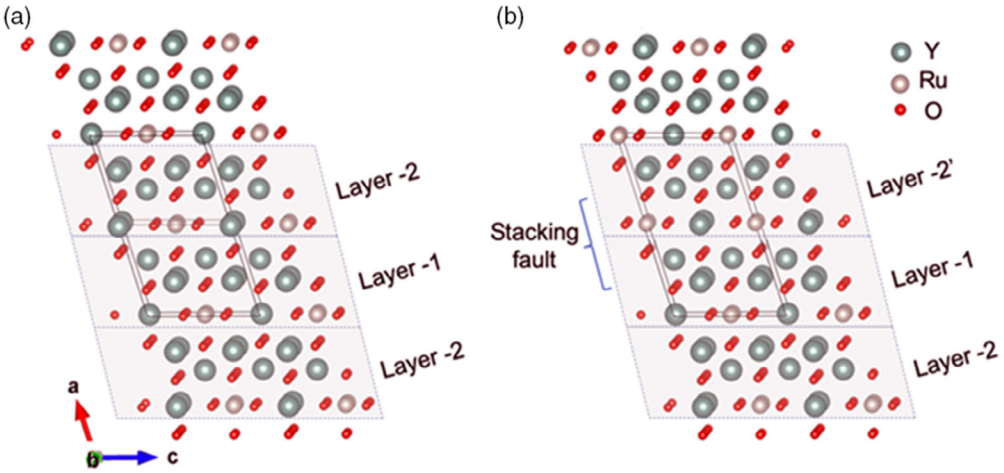

Figure 6. a) The ideal disorder-free structure and b) defect structures likely responsible for the observed diffuse streaks along the *H* direction.

two adjacent layers (Figure 6b). Thus, the crystal loses the long-range translation symmetry along the *a*-axis, which can give rise to the streak-like diffuse scattering features. Further, we find that simulations using other interlayer displacement vectors (including $\mathbf{t} = [1/2, 0, 0]$) do not agree with the presence of the observed streak-like features in our experiment. To test this idea, we performed simulations using the software package DISCUS[48] to calculate diffuse scattering patterns at multiple [*H* 0 0] and [0 *K* 0] planes with different *L* values. A relatively large stacking fault probability of 15% was used in the simulation. This was not aimed at quantitively explaining the scattering intensity but at qualitatively explaining the main diffuse scattering features. The simulation results are in good agreement with the main features of the diffuse scattering observed in our experimental data and further confirm the disordered structure of $Y_5Ru_2O_{12}$.

4. Conclusion

In this study, we demonstrate that the yttrium ruthenate, $Y_5Ru_2O_{12}$, can be grown as large, high-quality single crystals using a hydrothermal technique that allows us to grow these crystals at relatively lower temperatures (<700 °C) than the classical melt methods. The compound is a member of a known structure type with a formula of $Ln_5B_2O_{12}$ (Ln = Y, La–Lu; *B* = Mo, Ru, Re). Study of $Y_5Ru_2O_{12}$ is particularly interesting because it is based on the magnetically silent yttrium atom, allowing the magnetic contribution of the ruthenium sublattice to be carefully examined. The $Y_5Ru_2O_{12}$ structure contains edge-sharing Ru—O—Ru chains with alternating Ru—Ru shorter and longer distances, which are embedded in a Y—O—Y lattice. This alternating B—O—B distance in the chains is characteristic of this class of compounds. Single crystal neutron diffraction data confirm that the $Y_5Ru_2O_{12}$ is subject to stacking faults, probably due to the presence of Y, Ru, and O-site disorder that was modeled from the single crystal X-ray diffraction data. The formal oxidation state of the Ru ions is +4.5 and the magnetic property investigation of $Y_5Ru_2O_{12}$ indicates a short-range ordering due to the presence of Ru—O—Ru chains before antiferromagnetic order is induced below 30 K. The material possesses an anomalously large magnetic moment, which precludes the assignment of simple alternating Ru—Ru bonds in the dimers, as is observed for corresponding Re or Mo analogs. We propose a more complex scenario for a coupling interaction between Ru centers in the Ru-oxo chain as the reason for the higher effective magnetic moment observed in $Y_5Ru_2O_{12}$. Additional neutron diffraction data are warranted to confirm our structural model. This work demonstrates the importance of preparing single crystals sufficiently large for both oriented magnetic and single crystal neutron diffraction measurements. This compound represents another example of the complex and unconventional magnetic and orbital behavior of ruthenium oxides and demonstrates a viable route to additional metal ruthenates.

Supporting Information

Supporting Information is available from the Wiley Online Library or from the author.

Acknowledgements

The research at the Oak Ridge National Laboratory (ORNL) is supported by the USA. Department of Energy (DOE), Office of Science, Basic Energy Sciences (BES), Materials Sciences and Engineering Division (MSE). This research used resources at Spallation Neutron Source, a DOE office of Science User Facility operated by ORNL. The synthesis and single-crystal X-ray diffraction were performed at Clemson University and funded by the National Science Foundation under Grant DMR-1808371.

Conflict of Interest

The authors declare no conflict of interest.

Keywords

crystal growth, hydrothermal synthesis, magnetic ordering, neutron diffraction, ruthenium oxide

Received: April 2, 2020
Revised: August 27, 2020
Published online: September 21, 2020

[1] W. Witczak-Krempa, G. Chen, Y. B. Kim, L. Balents, *Annu. Rev. Condens. Matter Phys.* **2014**, *5*, 57.
[2] S. G. Ovchinnikov, *Phys. Uspekhi* **2003**, *46*, 46.
[3] R. J. Cava, *Dalton Trans.* **2004**, *19*, 2979.
[4] J. A. Sears, M. Songvilay, K. W. Plumb, J. P. Clancy, Y. Qiu, Y. Zhao, D. Parshall, Y. J. Ki, *Phys. Rev. B* **2015**, *91*, 144420.
[5] R. J. Bouchard, J. L. Gillson, *Mater. Res. Bull.* **1972**, *7*, 873.
[6] K. Ishida, H. Mukuda, Y. Kitaoka, K. Asayama, Z. Q. Mao, Y. Mori, Y. Maeno, *Nature* **1998**, *396*, 658.
[7] C. I. Hiley, D. O. Scanlon, A. A. Sokol, S. M. Woodley, A. M. Ganose, S. Sangiao, J. M. De Teresa, P. Manuel, D. D. Khalyavin, M. Walker, M. R. Lees, R. I. Walton, *Phys. Rev. B* **2015**, *92*, 104413.
[8] C. I. Hiley, M. R. Lees, J. M. Fisher, D. Thompsett, S. Agrestini, R. I. Smith, R. I. Walton, *Angew. Chem.* **2014**, *126*, 4512.
[9] T. Marchandier, W. Jacquet, G. Rousse, B. Baptiste, A. M. Abakumov, J.-M. Tarascon, *Chem. Mater.* **2019**, *31*, 6295.
[10] C. A. Marjerrison, C. Mauws, A. Z. Sharma, C. R. Wiebe, S. Derakhshan, C. Boyer, B. D. Gaulin, J. E. Greedan, *Inorg. Chem.* **2016**, *55*, 12897.
[11] C. I. Hiley, D. O. Scanlon, A. A. Sokol, S. M. Woodley, A. M. Ganose, S. Sangiao, J. S. De Teresa, P. Manuel, D. D. Khalyavin, M. Walker, M. R. Lees, R. I. Walton, *Phys. Rev. B* **2015**, *92*, 104413.
[12] A. Kanbayasi, *J. Phys. Soc. Jpn.* **1976**, *41*, 1876.
[13] P. Khalifah, K. D. Nelson, R. Jin, Z. Q. Mao, Y. Liu, Q. Huang, X. Gao, A. P. Ramirez, R. J. Cava, *Nature* **2001**, *411*, 669.
[14] D. Ziat, A. A. Aczel, R. Sinclair, Q. Chen, H. D. Zhou, T. J. Williams, M. B. Stone, A. Verrier, J. A. Quilliam, *Phys. Rev. B* **2017**, *5*, 184424.
[15] M. S. Senn, S. A. J. Kimber, A. M. A. Lopez, A. H. Hill, J. P. Attfield, *Phys. Rev. B* **2013**, *87*, 134402.
[16] P. Lightfoot, P. D. Battle, *J. Solid State Chem.* **1990**, *89*, 174.
[17] S. A. J. Kimber, M. S. Senn, S. Fratini, H. Wu, A. H. Hill, P. Manuel, J. P. Attfield, D. N. Argyriou, P. F. Henry, *Phys. Rev. Lett.* **2012**, *108*, 217205.
[18] K. E. Stitzer, M. D. Smith, W. R. Gemmill, H.-Z. zur Loye, *J. Am. Chem. Soc.* **2002**, *124*, 13877.
[19] H. W. Zandbergen, D. J. W. Ijdo, *Acta. Crystallogr.* **1984**, *C40*, 919.
[20] Q. Chen, S. Fan, K. M. Taddei, M. B. Stone, A. I. Kolesnikov, J. Cheng, J. L. Musfeldt, H. D. Zhou, A. D. Aczel, *J. Am. Chem. Soc.* **2019**, *141*, 9928.
[21] W. Miiller, M. Avdeev, Q. Zhou, A. J. Studer, B. J. Kennedy, G. J. Kearley, C. D. Ling, *Phys. Rev. B* **2011**, *84*, 220406.
[22] L. T. Nguyen, R. J. Cava, arXiv:2006.05864 [cond-mat.str-el], **2020**.
[23] M. S. Senn, A. M. Arevalo-Lopez, T. Saito, Y. Shimakawa, J. P. Attfield, *J. Phys.: Condens. Matter* **2013**, *25*, 496008.
[24] I. Terasaki, T. Igarashi, T. Nagai, K. Tanabe, H. Taniguchi, T. Matsushita, N. Wada, A. Takata, T. Kida, M. Hagiwara, K. Kobayashi, K. H. Sagayama, S. Kumai, H. Nakao, Y. Murakami, *J. Phys. Soc. Jpn.* **2017**, *86*, 033702.
[25] L. D. Sanjeewa, K. A. Ross, C. L. Sarkis, H. S. Nair, C. D. McMillen, J. W. Kolis, *Inorg. Chem.* **2018**, *57*, 12456.
[26] M. Powell, L. D. Sanjeewa, C. D. McMillen, K. A. Ross, C. L. Sarkis, J. W. Kolis, *Cryst. Growth Des.* **2019**, *19*, 4920.
[27] C. D. McMillen, L. D. Sanjeewa, C. A. Moore, D. C. Brown, J. W. Kolis, *J. Cryst. Growth* **2016**, *452*, 146.
[28] K. M. Taddei, L. D. Sanjeewa, J. W. Kolis, A. S. Sefat, C. de la Cruz, D. M. Pajerowski, *Phys. Rev. Mater.* **2019**, *3*, 014405.
[29] D. M. Pajerowski, K. M. Taddei, L. D. Sanjeewa, A. T. Savici, M. B. Stone, J. W. Kolis, *Phys. Rev. B* **2020**, *101*, 014420.
[30] K. Fulle, C. D. McMillen, L. D. Sanjeewa, J. W. Kolis, *Cryst. Growth Des.* **2016**, *16*, 4910.
[31] L. D. Sanjeewa, C. D. McMillen, J. W. Kolis, *Dalton Trans.* **2019**, *48*, 7704.
[32] K. Fulle, L. D. Sanjeewa, C. D. McMillen, C. R. De Silva, K. Ruehl, Y. Wen, G. Chumanov, J. W. Kolis, *J. Alloys Compd.* **2019**, *786*, 489.
[33] K. Fulle, L. D. Sanjeewa, C. D. McMillen, J. W. Kolis, *Dalton Trans.* **2018**, *47*, 6754.
[34] M. T. K. Kolambage, C. D. McMillen, M. A. McGuire, L. D. Sanjeewa, K. Ivey, Y. Wen, G. Chumanov, J. W. Kolis, *J. Solid State Chem.* **2019**, *275*, 149.
[35] M. T. K. Kolambage, C. D. McMillen, M. Ivey, J. W. Kolis, *J. Alloys Compd.*, to be published.
[36] M. Bharathy, W. R. Gemmill, A. H. Fox, J. Darriet, M. D. Smith, H.-C. zur Loye, *J. Solid State Chem.* **2009**, *182*, 1164.
[37] L. Chi, J. F. Britten, J. E. Greedan, *J. Solid State Chem.* **2003**, *172*, 451.
[38] D. M. Colabello, E. M. Sobalvarro, J. P. Sheckelton, J. C. Neuefeind, T. M. McQueen, P. G. Khalifah, *Inorg. Chem.* **2017**, *56*, 12866.
[39] C. C. Torardi, C. Fecketter, W. H. McCarroll, F. J. DiSalvo, *J. Solid State Chem.* **1985**, *60*, 332.
[40] Apex3, Bruker AXS Inc., Madison, WI, **2015**.
[41] G. M. Sheldrick, *Acta Crystallogr. A: Found. Crystallogr.* **2008**, *64*, 112.
[42] L. Shlyk, S. Strobel, E. Rose, R. Niewa, *Solid State Sci.* **2012**, *14*, 281.
[43] F. Ye, Y. Liu, R. Whitfield, R. Osborn, S. Rosenkranz, *J. Appl. Crystallogr.* **2018**, *51*, 315.
[44] T. M. Michels-Clark, A. T. Savici, V. E. Lynch, X. Wang, X. M. Chodkiewicz, T. Weber, H. Bürgi, C. M. Hoffmann, *J. Appl. Crystallogr.* **2017**, *50*, 1559.
[45] A. J. Cortese, D. Abeysinghe, B. Wilkins, M. D. Smith, G. Morrison, H.-C. zur Loye, *Inorg. Chem.* **2015**, *54*, 11875.
[46] L. Shlyk, K. Nenkov, B. Schupp-Niewa, G. Krabbes, G. Fuchs, *Phys. Rev. B* **2006**, *74*, 054428.
[47] M. Itoh, M. Shikano, T. Shimura, *Phys. Rev. B* **1995**, *51*, 16432.
[48] T. Proffen, R. B. Neder, *J. Appl. Crystallogr.* **1997**, *32*, 171.